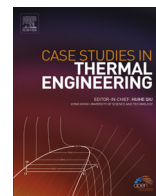




Contents lists available at ScienceDirect

Case Studies in Thermal Engineering

journal homepage: www.elsevier.com/locate/csite

Effects of mist fractions on heat transfer characteristics in a rotating roughened cooling passage



Hamad M. Alhajeri^{a,*}, Abdulrahman H. Alenezi^a, Abdulrahman Almutairi^a,
M.H. Alhajeri^a, Abdalaziz A.A. Gamil^b

^a Mechanical Power and Refrigeration Technology Department, College of Technological Studies, PAAET, Shuwaikh, Kuwait

^b Department of Power and Propulsion, Cranfield University, Cranfield, Bedfordshire, MK43 0AL, UK

ABSTRACT

This paper investigates the effects of the mist fractions on heat transfer characteristics applied on a rotating U-channel with inclined ribs at an angle of 45°. This study has been conducted on five different mist percentages from 1 to 5 with a 1% increment at each step, and all of the cases have been investigated for Reynolds number values of 5000, 10000, 25000 and 40000. The numerical results obtained from the application of RNG k-ε turbulence model with enhanced-wall function were in good agreement with the experimental data of the smooth and ribbed channels both with and without mist addition. Results also demonstrated a 300% increase in the flow temperature difference and a noticeable increase in Nusselt number at each bend region and at the downstream of the leading edge around 25% and 110% respectively, at high mist fraction (5%); when compared with the case where only air was used. With %5 mist addition, the convective efficiency also reaches approximately 69%.

1. Introduction

New methods of cooling techniques for gas turbine blades have been developed with the advancements of gas turbine technology. The current cooling techniques can be divided into two main categories, internal and external cooling. Internal cooling methods mainly focus on jet impingement or extended surfaces to improve the heat transfer by increasing the area between the blade surface and the cooling fluid. An example for external cooling is air film cooling, which is a conventional external cooling method. The techniques that has been currently used are unfortunately limited in terms of cooling performance, and it is very clear that new approaches are required to increase the effectiveness of cooling beyond current restrictions.

Usually, compressed air first passes through the combustor and then is channelled through turbine blades for cooling in traditional cooling methods. The air enters the turbine rotor and exits from trailing edge of turbine blades where it meets with hot gasses. The turbine blades are subjected to thermal stress as hot blade surfaces are cooled down with bleed air. Mist air has been used as a working fluid on recent studies to improve cooling on gas turbines.

Fine water droplets in the form of a mist are diffused into the cooling air stream in order to improve cooling performance [1–3]. This method does not generate a substantial change in the extracted air from the compressor. This method uses the water at latent heat, which is higher than air to provide cooling with the mist. The heat transfer rate between the coolant and the hot surface increases with the usage of high latent heat [4–11]. Cooling efficiency would increase as the mist would evaporate near the hot surface and absorb more heat, which is considered as a distinctive feature of the mist-air mixture [12–14].

Studies conducted by Refs. [15–20] have investigated mist steam cooling in a heated circular stainless steel tube, on a 180-degree bend, with an impingement jet on a flat surface and an impingement jet over a curved surface. These studies demonstrated improvements in cooling performance which has reached up to 100% for when the steam is between the flow phase and mist/steam

* Corresponding author.

E-mail address: hmhajeri@gmail.com (H.M. Alhajeri).

<https://doi.org/10.1016/j.csite.2019.100506>

Received 20 June 2019; Received in revised form 23 July 2019; Accepted 25 July 2019

Available online 30 July 2019

2214-157X/© 2019 The Authors. Published by Elsevier Ltd. This is an open access article under the CC BY-NC-ND license

(<http://creativecommons.org/licenses/by-nc-nd/4.0/>).

| Nomenclature | | | |
|-------------------|---|--------------|--------------------------------------|
| A | Area (m^2) | w | Wall |
| C | Concentration of species | v | Vapor |
| D | Diameter (m) | vm | Virtual mass force |
| D_v | Diffusivity | Nu | Nusselt Number |
| F | Force ($kg/m^2 s^2$) | p | Static pressure (Pa) |
| f | Molar fractions | Pr | Prandtl number |
| h | Heat transfer coefficient ($W/m^2 K$) | \dot{q} | Wall heat flux (W/m^2) |
| I | Enthalpy (J/kg) | Re | Reynolds number (–) |
| k | Thermal conductivity ($W/m \cdot K$) | Sc | Schmidt number (–) |
| L | Length (m) | S_m | Source term of mass ($kg/m^3 s$) |
| m | Mass (kg) | S_h | Source term of energy ($J/m^3 s$) |
| M | Molecular weight | s_i | Source term of species ($N s/m^3$) |
| Subscripts | | Sh | Sherwood number |
| b | Bulk | T | Temperature (K) |
| fg | Latent heat | u | Velocity (m/s) |
| h | Hydraulic | Greek | |
| i | Inlet | Δ | Difference (–) |
| o | Outlet | η | Convective efficiency (–) |
| p | Particle or droplet | ρ | Density (kg/m^3) |
| | | μ | Molecular viscosity ($N m/s^2$) |
| | | τ | Viscous shear stress tensor (Pa) |

mixtures. In addition, local heat transfer has reached around 200% when the droplets have 5% mass ratio [21] has investigated pulsed jet impingement with mist droplets and has concluded that heat transfer increases by increasing pulsed frequency.

Torfeh and Kouhikamali [22] have conducted numerical investigations for injecting mist into vapor using Discrete Phase Model (DPM), the geometry that has been used was a vertical tube with a smooth wall [22] have found when thermal equilibrium takes place, the rate of the heat transfer between the flow and mist droplets occurs so rapidly that the flow temperature remains saturated. They have also indicated that when there is thermal equilibrium heat transfer takes place too slowly from the flow to the mist particles.

Elwekeel et al. [23] have investigated the effects of coolants on the flow and heat transfer characteristics of both rotating and non-rotating channels with ribs at angles of 45° and 90°, and it has been indicated that the mist/steam have given the best results in terms of the performance of heat transfer. In their studies, Feng Zhang, demonstrated that water particles travel through greater distances with rotation effect at low Reynolds numbers, while when the flow has high Reynolds numbers rotation has insignificant effects on the particles.

The literature survey has demonstrated that the previous studies on this topic have mainly focused on using a fixed value of mist concentration in cooling passages. The current research on this topic do not investigate the relation between heat transfer characteristics and the mist concentration and rotation. This paper investigates the effects of different mist concentrations on heat transfer characteristics, such as the Nusselt number, flow average temperature, and convective efficiency. The used geometry for this investigation is a rotating two-pass roughened rectangular channel.

2. Methodology

The simulation of the interaction between the water particles in the air and the evaporation mechanism has been completed by using a two-phase modelling approach. For two-phase modelling, continuous phase and discrete phase has been used, the air has been modelled as continuous phase and the mist is modelled as discrete phase in the used CFD code. The most important criteria of this two-phase mechanism were to ensure modelling of the water evaporation, which was formed by air and water vapor. The numerical modelling approach has been explained below.

The water mass fraction usually changes between 1 and 5% of air mass flow rate during the use of DPM and it is limited in terms of mist concentration in the air. This statement is valid for the used flow condition. The continuous phase modelling has been completed by Eulerian model and trajectory calculations of the water particles has been completed with Lagrangian model during the numerical calculations. The interaction between the discrete phase (water droplets) and the continuous phase (air) were calculated with source terms for mass, momentum, energy and species concentrations.

2.1. Continuous phase

The RANS (Reynolds Averaged Navier-Stokes) equations for conservation of mass, momentum, energy and species are given as the followings:

Continuity equation:

$$\nabla \cdot (\rho u) = s_m \quad (1)$$

Momentum equation:

$$\nabla \cdot (\rho uu) = -\nabla p + \nabla \cdot (\bar{\tau}) + F \quad (2)$$

Energy equation:

$$\nabla \cdot \left(\rho u \left(e + \frac{u^2}{2} \right) \right) = \nabla \cdot (k \nabla T + (\bar{\tau} \cdot u) - up) + u \cdot F + S_h \quad (3)$$

Species equation:

$$\nabla \cdot (uc) = \nabla \cdot (D \cdot \nabla c) + S_i \quad (4)$$

The source term S_m represents the mass transfer from the dispersed second phase to the continuous phase caused by vaporization of liquid droplets, S_h represents the heat source and s_i represents the source term of this species. ρ and u represents the density of continuous phase, respectively. p is static pressure, $\bar{\tau}$ is the viscous shear stress tensor, e and $u^2/2$ are flow of internal and kinetic energy, respectively. k is thermal conductivity, c is the concentration (mass fraction) of species and D is the diffusion coefficient.

2.2. Discrete phase

The motion of the particles can also be simulated in the Lagrangian frame for discrete phase as well as solving the transport equations for the continuous phase. The liquid in the mist is modelled as spherical particles which are allowed to diffuse in the continuous phase in the Lagrangian frame. The motion of the particles can be described by the below equation,

$$du_p/dt = F_D(u - u_p) + \frac{g_x(\rho_p - \rho)}{\rho_p} + F_{vm} + F_x \quad (5)$$

On the above equation, $F_D(u - u_p)$ represents the drag force per unit particle mass $\frac{g_x(\rho_p - \rho)}{\rho_p}$ represents the gravity force per unit mass, F_{vm} represents the virtual mass force per unit mass and F_x represents the additional forces such as pressure gradient, thermophoretic and a rotating reference frame. g_x represents the gravitation acceleration, ρ and ρ_p represents the fluid density and the particle density, respectively. u and u_p represent fluid phase velocity and the particle velocity.

The particle temperature has been changed based on the relation between the sensible heat change in the particle and the convective and the latent heat transfer between the particle and the continuous phase. In this case, the energy balance equation would give the rate of the particle temperature change.

$$\frac{d(m_p \cdot T_p \cdot C_w)}{dt} = A_p k Nu_p (T - T_p) + \frac{dm_p}{dt} I_{fg} \quad (6)$$

Here, m_p represents the particle mass, A_p represents the surface area of the particle, T represents the temperature of the continuous phase, T_p represents the droplet temperature, $\frac{dm_p}{dt}$ represents the rate of evaporation and I_{fg} represents the latent heat. The empirical correlation of Nu_p can be obtained from [26]:

$$Nu_p = 2 + 0.6 Re_p^{0.5} (\mu C_p / k)^{0.33} \quad (7)$$

Here, Nu_p and Re_p represent the particle's Nusselt number and Reynolds number, respectively. The gradient diffusion, which regulates the mass transfer rate; includes the particle vapor flux into the gas phase which is related to the gradient of the vapor concentration between the droplet surface and the bulk gas is given below:

$$\frac{dm_p}{dt} = -A_p k Nu_p (T - T_p) / I_{fg} \quad (8)$$

The rate of mass transfer is as indicated below when the particle is below the boiling point,

$$\frac{dm_p}{dt} = A_p \rho_v D_v Sh \left(\frac{M_v}{M} \right) \log \left[\frac{1 - f_p}{1 - f} \right] \quad (9)$$

Here, ρ_v and D_v represent the density and diffusivity of the vapor respectively, Sh represents the Sherwood number which is defined as the ratio between mass transfer by convection and mass transfer by diffusion. M_v and M represent, the molecular weight of the vapor and the mixture in continuous phase, respectively and lastly f_p and f represent the molar fractions of the particle and the gas phase respectively. Sh is given by the equation below.

$$Sh = 2 + 0.6 Re_p^{0.5} Pr^{0.3} \quad (10)$$

3. Computational domain and boundary conditions

The computational model in this study is adopted from Ref. [25]. The proposed model configuration is widely used in the literature because of its almost identical to the geometry of the internal channel configuration for a gas turbine blade in the sake of evaluating the heat transfer enhancement. The geometry has been described in Fig. (1-a), with two pass square cross section of 12.7 mm * 12.7 mm and a 180° sharp bend. Starting from the opening of the square channel, there is an unheated section 558 mm in length. A heated section of 152.4 mm has been provided for the calculation of the turbine blade heat flux, with ribs at an angle of 45° to the flow. A number of ribs have been installed on the internal top and bottom surfaces and they are heated at a constant heat flux, while sides have been designed as adiabatic walls and they do not contribute to the heat transfer. The top and bottom walls have ribs as turbulators to increase turbulence and heat transfer. Except the bend, the square channel has a constant aspect ratio. The square ribs are designed as 1.59 mm * 1.59 mm with a pitch to height ratio of 10 and they are placed at an angle of 45° to the flow.

The commercial CFD program used is ANSYS Fluent, and for the ribbed channels; mesh has been created with ICFM CFD module. With the refinements around ribs and the bend region, a fine mesh created with approximately 2.5 million cells. For the wall, the mesh is refined to keep y^+ less than 1. (Fig. 1-b) demonstrates the ribbed channel structured grid.

The two ribbed sides have been heated at a constant 4800 W/m² in the two-pass rib channel. The rotational speed of the channel is 550 RPM and the inlet air has been defined as ideal gas at 300 K. The analysis has been conducted for the Reynolds number of 5000, 10000, 25000 and 40000. For the discrete phase, mass fractions from 1% to 5%, with an increment of 1% has been investigated, and the particle diameter has been chosen as 6 μm. During the movement of the particle, it is expected that the particle might reflect, escape or evaporate from the boundary surface or be declared as incomplete. These set of possibilities are identified as the 'fate of particle'. In Ref. [25], the set of possibilities mentioned above have been explained. The unheated side walls are defined as adiabatic walls with non-slip velocity boundary condition. The inlet boundary condition turbulence intensity is defined as 2%. While the outlet is assumed to be at a constant pressure of 1.0 atm.

The pressure based segregated solver together with SIMPLE pressure velocity coupling algorithm is used and variable properties are defined as a function of temperature and pressure. The velocity values at the inlet have been calculated using the defined Reynolds numbers. As indicated above, the chosen Reynolds numbers were 5000, 10000, 25000 and 40000. The used commercial CFD program for the mesh sensitivity studies, turbulence model validation and simulations is Ansys Fluent.

The convective terms and turbulence terms were solved with high-order discretization accuracy. The convergence criterion for continuity, momentum equations, energy and turbulent kinetic energy is chosen less than 10⁻⁶. To ensure the convergence of the analyses, the total outlet temperature is observed. For all of the cases, the averaged Nusselt numbers obtained from the leading and trailing ribbed walls along with the defined Reynolds numbers, have been monitored.

The calculation of the heat transfer coefficient (h) and the Nusselt number has been completed with the following equations [24].

$$h = \dot{q}/(T_w - T_b) \quad (11)$$

$$Nu = \frac{hD_h}{k} \quad (12)$$

Here h is heat transfer coefficient; D_h is hydraulic diameter of a square channel and is equivalent to width or height of inlet surface; \dot{q} is heat flux of 4800 W/m²; T_w is average wall temperature of the heated walls; T_b is average bulk temperature of air. Thermal conductivity of the coolant is denoted by k . Another comparison is convective efficiency, η , can be expressed as follows:

$$\eta = \frac{T_o - T_i}{(T_w - T_i)} \quad (13)$$

where, T_o and T_i are outlet temperature and inlet temperature, respectively.

4. Results and discussion

4.1. Validation of the models

In order to validate the results obtained, the experimental study results obtained from Ref. [25] have been used. The grid was refined near the extended surfaces in order to ensure that the flow field in these regions accurately captured. Mesh dependency study

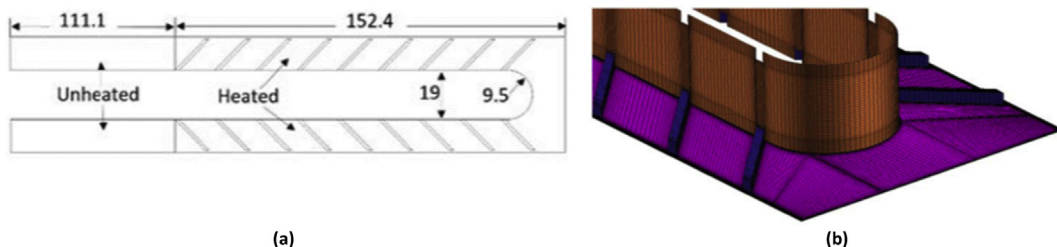


Fig. 1. (a) Rough U-Tube Geometry (b) Structured mesh for ribbed channel.

was carried to verify the computational model and mesh independency. The heated wall of the smooth U-tube has been exposed to a heat flux of 3800 W/m^2 , and the inlet steam saturated temperature was 385 K . Standard K- ϵ , RNG K- ϵ and k- ω SST turbulence models have been used in the analyses and the validation has been completed using the experimental results of [25]. Fig. 2 demonstrates the results obtained from the Nusselt number calculations of the mist/stem inside the smooth U-tube. The results obtained are in a good agreement at low Reynolds number, while at high Reynolds numbers the results overshoot/undershoot the experimental data results within a $\pm 5\%$ range. For this study, the RNG k- ϵ model with enhanced-wall function is used as the most accurate results have been obtained when compared with the experimental data and the results obtained from other turbulence models.

As can be seen in Fig. 3, the accuracy of the turbulence model has been evaluated with the measured values of the Nusselt number for non-rotating, air-only cases at different Reynolds numbers both in ribbed and smooth channel. This comparison demonstrates the accuracy of the turbulence model on the Nusselt number calculation. The results obtained from the smooth channel are in a good agreement, while the ribbed channel results gave under-predicted results especially at higher Reynolds numbers. The accuracy of the CFD code drastically reduces as the flow becomes more complex with the use of the ribs and at higher Reynolds numbers. As a summary, the difference between the results obtained from the experimental data and the numerical data are on an acceptable level, especially at the roughened channel when low Re values are used. The cooling efficiency has increased with the usage of the ribbed channel, as the surface area and the mixing ratio is greater.

4.2. Effects of mist fraction on heat transfer

The second part of this study covers heat transfer enhancement by injecting water droplets into the air. The injection of water mist was modelled using discrete phase model DPM. The Lagrange approach is used for the discrete phase with droplets as particles. The water mass fraction is considered of 1%, 2%, 3%, 4% and 5% of air mass flow rate. The mass flow rate of air for Re 25000 is 0.0056 kg/sec based on the hydraulic diameter. The post processing of particle tracking data allows the user to display the particles represented by a number of particle variables; including particle diameter, mass, temperature, velocity and other parameters. The maximum diameter size corresponds to an initial size of $5 \mu\text{m}$ for injection. The size of droplets decreases with temperature and droplets are evaporated at vaporization temperature. The minimum diameter is the limit set by the solver, below which the droplet is considered evaporated and mixed with the continuous phase. The mass of droplets also shows same behaviour of gradually decreasing in mass.

The flow average temperature along leading-edge surface was presented in Fig. 4 (a). The plot conducts at several of mist fraction for first passage (1–8) and the second passage (8–16). The several small temperature peaks occur at both first and second passages of the channel. However, a noticeable peak occurs at location 8 where the 180-degree turn takes place causing small scales of recirculation. The upstream inlet flow temperature has shown an increase in temperature with the distance away from the inlet location due to continues heat transfer with the heated wall. As the mist/air ratio increases, the airflow temperature increases due to the existence of water droplets. Similar behaviour can be noticed in the second passage. The temperature difference increases by almost 450% comparing to temperature of single phase (air) between locations 8 and 16 at 5% mist. For the overall passage, the use of 5% mist can achieve 300% more heat absorption than air only case.

Fig. 4 (b) shows the averaged Nusselt number predicted at the downstream of the ribs on the leading-edge surface at various mist ratios. For single phase flow, the Nusselt number increases from 150 to 170 with a percentage of 13% at location 4 and reduces to 140 at location 8 before rises to 170 at location 9, finally reduces to 140 at the last location. The 180-degree bend at location 9 has caused increasing of Nusselt number on the leading edge when centrifugal force is forcing more airflow acting on the leading surfaces locally, which greatly assist in cooling enhancement on these surfaces. This pattern remains the same and with more significance for the mist cooling. Compared to only 25% of Nusselt number jumps to the bend region and 110% of Nusselt enhances by 5% mist at the end of leading edge. At 5% mist fraction, the dropping values of Nusselt number at upstream and downstream are 150–293, respectively.

Nusselt number surface contours of the trailing and leading edges at different mist/air ratio were shown in Fig. 5. When no mist is used for the inlet trailing edge, the Nusselt number increasing in rib downstream regions until the fourth rib location as shown in

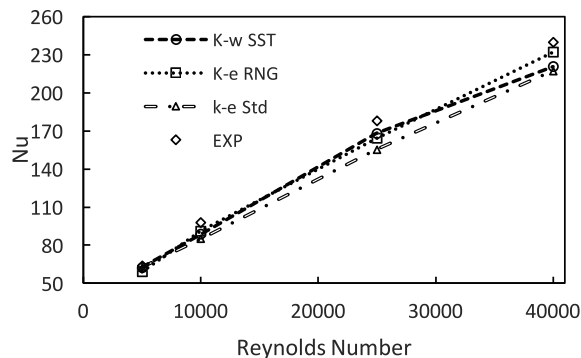


Fig. 2. Comparison of turbulence model for heat transfer studies in smooth U tube with experimental data [25].

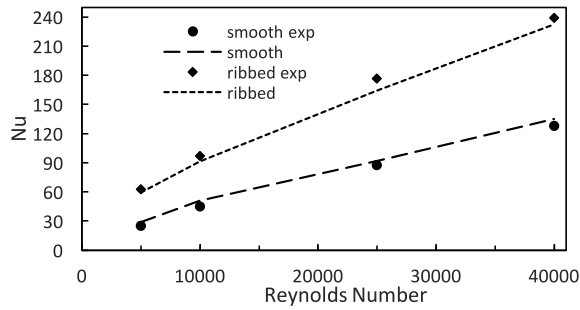


Fig. 3. Validation of CFD Model for smooth and ribbed passage with experimental data [25].

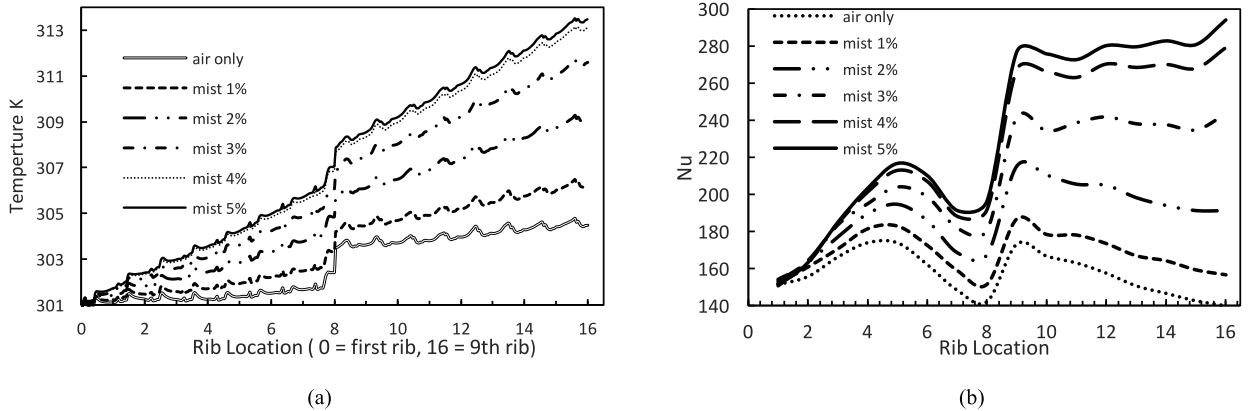


Fig. 4. (a) Flow average Temperature on leading edge surface (b) Averaged Nusselt number downstream of the ribs on leading edge surface.

Fig. 5 a. Nusselt value is at its peak before reducing towards the outlet. Then it's reduced until it reaches the last rib at the outlet. In between 1% and 3% mist ratios, the Nusselt number distribution also shows consistent with the trend that shifting of the peak Nusselt region from as early as 4th rib location towards 5th rib at the first passage. While at mist fractions 4% and 5%, Nusselt number peak reach the middle of the second passage.

Overall, first passage shows more heat transfer as a result of the high Nusselt number, this is the case for air and mist up to 3%, but as mist fraction increases, the high Nusselt number shift to the second passage as shown in Fig. 5, further more when 5% mist/air ratio injected in with the flow, the Nusselt number has moved its peak at the outlet passage. Heat transfer is significantly higher at the second passage for the 4% and 5% mist. In term of consistency heat transfer is uniform along the second passage for cases with mist ratios from 3% to 5%. It's clear that the case of 0%–2% mist, heat transfer increasing towards the centre of the first passage then decreases gradually. At 3% mist is the only case where the inlet and outlet trailing passage close to each other in respect of heat transfer.

Fig. 5 b shows the distribution of Nusselt number on the leading edges wall of the 180 deg duct. As compared to the distribution on the trailing edge (Fig. 5 a), in cases of air only and 1% mist, first passage shows more heat transfer while cases 2%–5% mist shows high heat transfer in the second passage. Also, the second passage in cases 4% and 5% mist demonstrates high heat transfer approximately double the first passage.

Fig. 6 (a) shows the overall averaged Nusselt number variations with mist/air ratio for leading and trailing passages. Mist/air ratios of 1%–5% was injected at inlet roughness channel with droplet diameter of 6 μm. From this figure, can be seen that the heat transfer was much higher on the second passage compared to the first passage at high mist/air ratio. While the trends show adverse directions at low mist/air ratio [22]. Due to high mist fraction and rotational, the droplets are subjected to the effect of centrifugal and Coriolis forces and these forces move the droplets to trailing edge.

The leading edge of the second passage shows great enhancement with the increases of mist/air, where Nusselt number values are 145 and 248 for air only and 5% mist, respectively. While the leading edge of the first passage shows less enhancement with the increasing of mist/air.

In addition, For the first and the second passage trailing edges there was a small difference in Nusselt number between 4% and 5% mist which mean the heat enhancement was very little after 4% mist similar observation was found by Ref. [23]. That is due to rotation, which helps to absorb more heat and evaporation the droplets. The Nusselt number on the first passage surfaces increases in slower rate as mist/ratio increasing beyond 1%. For the second passage wall surfaces (leading and trailing), Nusselt number has surpassed the first passage one after mist/air ratio 3.5%.

Fig. 6 (b) shows the averaged Nusselt number of total wall surfaces at different mist/air ratio. It's clear that as mist/air ratio increases, Nusselt number also increases. The Nusselt number increases by 12.5% at doubling the mist/air ratio from 1% to 2% and

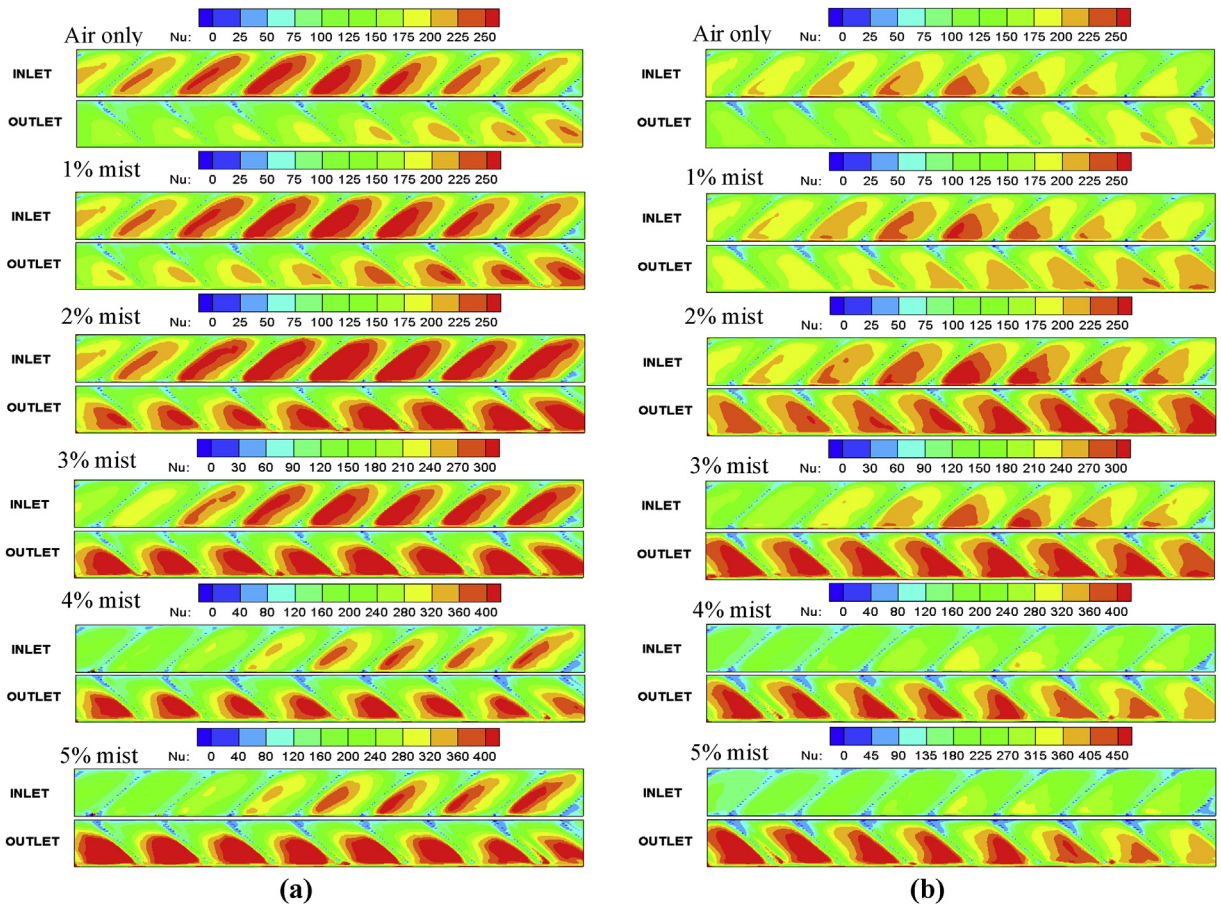


Fig. 5. Nusselt number distribution of both first and second passages (a) Trailing edge, (b) Leading edge.

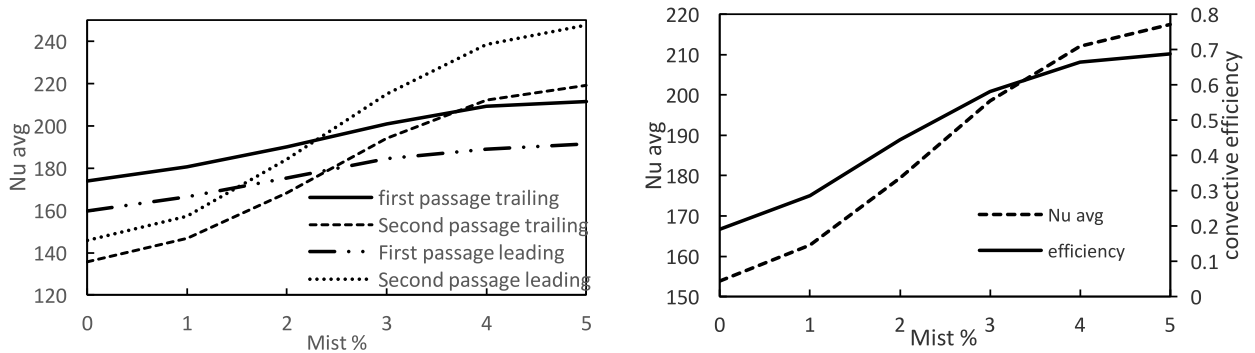


Fig. 6. (a) Averaged Nusselt number variations with mist/air ratio at both first and second passage walls surfaces (b) Average Nu values with mist injection.

increasing until reach 4% then it increases gradually. Overall, the total average Nusselt number has increases by almost 41% when 5% mist is used. Fig. 6 (b) also shows the averaged convective efficiency predicted at various mist/air ratios. It is clear that as mist/air ratio increases, the convective efficiency will increase. The convective efficiency reaches 69% at 5% mist addition.

5. Conclusion

In this Study, A numerical analysis was carried to investigate the impact of mist fraction on heat transfer on rotating cooling channel.

A CFD model was developed to investigate the effect of mist/air ratios on heat transfer in rotating cooling passage. The following

conclusions are extracted.

- For both smooth and rough passage cases, there is a good correlation between results obtained from K epsilon RNG turbulence model and empirical data.
- Varied mist percentages are compared based on the characteristics of distribution of particulates concentration without considering the concentration ratio. There is significant concentration of particles around the ribs causing an increased heat transfer. Particle trapped in the ribs circulation zone result in increase in Nusselt number.
- Mist ratio from 3% to 5% moved the maximum heat transfer area from the upstream passage to the downstream passage.
- Cooling enhancement in the leading edge accomplished with mist injection, Nusselt number increased from 150 to 295 (97% enhancements). Heat transfer increased with mist percentages until mist percentage of 4% then it increased gradually.

Acknowledgment

The authors acknowledge the valuable support and assistance provided by Public Authority for Applied Education and Training (PAAET), in state of Kuwait, through the financial support under project no. TS-19-01.

References

- [1] X. Li, T. Gaddis, T. Wang, J.L. Gaddis, T. Wang, Mist/steam heat transfer in confined slot jet impingement, *ASME J. Turbomach.* 123 (1) (2001) 161–167.
- [2] M. A. a. Pakhomov, V.I.I. Terekhov, Enhancement of an impingement heat transfer between turbulent mist jet and flat surface, *Int. J. Heat Mass Transf.* 53 (15–16) (Jul. 2010) 3156–3165.
- [3] M. A. a. Pakhomov, V.I.I. Terekhov, The effect of confinement on the flow and turbulent heat transfer in a mist impinging jet, *Int. J. Heat Mass Transf.* 54 (19–20) (Sep. 2011) 4266–4274.
- [4] M. Trela, An approximate calculation of heat transfer during flow of an air-water mist along a heated flat plate, *Int. J. Heat Mass Transf.* 24 (4) (1981) 749–755.
- [5] P.J. O'Rourke, Collective Drop Effects on Vaporizing Liquid Sprays, Princeton University, 1981.
- [6] Y. Mori, K. Hijikata, T. Yasunaga, Mist cooling of very hot tubules with reference to through-hole cooling of gas turbine blades, *Int. J. Heat Mass Transf.* 25 (9) (1982) 1271–1278.
- [7] P.J. O'Rourke, A.A. Amsden, The Tab Method for Numerical Calculation of Spray Droplet Breakup, SAE Tech. Pap., 1987.
- [8] S.L. Lee, Z.H. Yang, Y. Hsyua, Cooling of a heated surface by mist flow, *J. Heat Transf.* 116 (1) (1994) 167–172.
- [9] K.M. Graham, S. Ramadhyani, Experimental and theoretical studies of mist jet impingement cooling, *J. Heat Transf.* 118 (2) (1996) 343–349.
- [10] H. Barrow, C.W. Pope, Droplet evaporation with reference to the effectiveness of water-mist cooling, *Appl. Energy* 84 (4) (2007) 404–412.
- [11] T. Wang, X. Li, Mist film cooling simulation at gas turbine operating conditions, *Int. J. Heat Mass Transf.* 51 (21–22) (2008) 5305–5317.
- [12] N. Kumari, et al., Analysis of evaporating mist flow for enhanced convective heat transfer, *Int. J. Heat Mass Transf.* 53 (15–16) (Jul. 2010) 3346–3356.
- [13] M.Q. Brewster, Evaporation and condensation of water mist/cloud droplets with thermal radiation, *Int. J. Heat Mass Transf.* 88 (Sep. 2015) 695–712.
- [14] M. A. a. Pakhomov, V.I.I. Terekhov, Second moment closure modelling of flow, turbulence and heat transfer in droplet-laden mist flow in a vertical pipe with sudden expansion, *Int. J. Heat Mass Transf.* 66 (Nov. 2013) 210–222.
- [15] T. Guo, T. Wang, J.L. Gaddis, Mist/steam cooling in a heated horizontal tube-Part 1: experimental system, *J. Turbomach.* 122 (2) (2000) 360–365.
- [16] T. Guo, T. Wang, J.L. Gaddis, Mist/Steam Cooling in a Heated Horizontal Tube — Part 2: Results and Modeling vol. 122, (2000) April 2000.
- [17] T. Guo, T. Wang, J.L. Gaddis, Mist/steam cooling in a 180-degree tube bend, *J. Heat Transf.* 122 (4) (2000) 749–756.
- [18] T. Wang, J.L. Gaddis, X. Li, Mist/steam heat transfer of multiple rows of impinging jets, *Int. J. Heat Mass Transf.* 48 (25–26) (Dec. 2005) 5179–5191.
- [19] X. Li, J.L. Gaddis, T. Wang, Mist/steam cooling by a row of impinging jets, *Int. J. Heat Mass Transf.* 46 (12) (Jun. 2003) 2279–2290.
- [20] X. Li, J.L. Gaddis, T. Wang, Modeling of heat transfer in a mist/steam impinging jet, *J. Heat Transf.* 123 (6) (2001) 1086.
- [21] M.A. Pakhomov, V.I. Terekhov, RANS modeling of flow structure and turbulent heat transfer in pulsed gas-droplet mist jet impingement, *Int. J. Therm. Sci.* 100 (2016) 284–297.
- [22] S. Torfeh, R. Kouhikamali, Numerical investigation of mist flow regime in a vertical tube, *Int. J. Therm. Sci.* 95 (2015) 1–8.
- [23] F.N.M. Elwekeel, A.M.M. Abdala, Q. Zheng, Heat Transfer and Flow Characteristics in 90 Deg Ribbed Duct Using Different Coolants, (2013), pp. 1–10.
- [24] A. Rasool, A. Qayoum, Numerical analysis of heat transfer and friction factor in two-pass channels with variable rib shapes, *Int. J. Heat Technol.* 36 (1) (2018) 40–48.
- [25] W.-L.-L. Fu, L.M. Wright, J.-C.-C. Han, Rotational buoyancy effects on heat transfer in five different aspect-ratio rectangular channels with smooth walls and 45 degree ribbed walls, *J. Heat Transf.* 128 (11) (2006) 1130–1141.